AD/RHIC/RD-116

RHIC PROJECT

Brookhaven National Laboratory

Vacuum System Performance for the First Sextant Test of the Relativistic Heavy Ion Collider

R. Davis, H. C. Hseuh, D. Pate, L. Smart, R. Todd, D. Weiss

October 1997

I. INTRODUCTION

One of the major milestones during the construction of the Relativistic Heavy Ion Collider (RHIC) is the completion and successful testing of the first one sixth of the ring. This report summarizes the performance of the vacuum systems as it relates to the First Sextant Test (FST), and the design changes which precipitated. Primary system testing included: *a)* the construction and commissioning of the cold-bore, warm-bore, insulating vacuum, and instrumentation and control systems, *b)* the method of locating helium leaks along the 493m long continuous insulating vacuum system, *c)* the measurement of helium absorption capacity of activated charcoal in the insulating vacuum, and *d)* the helium wave propagation inside the cold bore beam tubes.

The vacuum requirements necessary for transporting a *"one shot"* beam through the first sextant is more relaxed than storing a beam in the machine for ten hours or more. However, this paper will focus on the success of the FST relative to it's ultimate objective. There were no first order problems with the vacuum hardware or control architecture. However, there were several areas that required revision to improve overall performance. These revisions will be described fully.

II. CONSTRUCTION AND COMMISSIONING OF VACUUM SYSTEMS

Insulating Vacuum System

The first sextant insulating vacuum consists of six sections of variable length, the two triplets (D0-Q3 plus transfer lines to the long arcs), the inner blue 493 meter arc (BI5DU3-BI4Q4), and three sections (YO5DU3-YO5Q7, YO5Q8-YO5Q9, YO5D9-YO4Q4) that comprise the outer yellow 493 meter arc.

The long arcs were constructed in strings of eight to thirteen magnets. Each string received vacuum checks on the cold bore beam line and all process lines. The magnet interconnect bellows were checked with vacuum tight fixtures which gave far greater sensitivity than using a sniffer. Once the interconnects were welded closed, an external leak check of the cryostat was completed, as well as an internal check with the coldmass slightly pressurized. These magnet strings were then joined and the entire cryostat pumped down. The remaining interconnects received an external leak check. Due to time-of-flight problems and helium attenuation within the cryostat, it was found beneficial to locate the pump and leak detector in close proximity to the area being leak checked. Finally, an internal pressure check was done on all process lines as well as the cold mass. It was found that when large external air leaks existed along the cryostat, a pressure gradient could be measured using the thermocouple (TCG)gauges. This proved beneficial in locating gross air leaks. As a result, additional TCGs will be added to the cryostats in the future to improve diagnostics and monitoring of the insulating vacuum. It was also found that hydrogen-deuterium (HD) worked well in finding small external leaks in cases of high helium background (i.e., magnets at 4.4°K).

Preliminary work was done on both the outgassing rate of the multi-layer insulation (MLI)[1] and the expected pumpdown of a 480 meter cryostat.[2] The estimates for the pumpdown of the cryostats proved optimistic. The test conditions during the out-gassing tests of the MLI did not accurately reproduce those found in the cryostats. The outgassing test sample was loosely rolled and only ~2 meters long. Conversely, the MLI in the cryostat is compressed and is longitudinal contiguous over its length. As a result, the MLI in the cryostat acts more like a virtual leak for water vapor leading to increased pump maintenance due to suspended water in the pump oil. The high pressure also decreases the sensitivity of room temperature leak checking of the cryostats.

A technique of pumping and purging was established to accelerate the outgassing of ~40 liters of water within each long cryostat. A pumpdown curve for a 13 magnet string is shown in Figure 1. It clearly shows an improved pumpdown slope after the first purge cycle. During the pumpdown, the water trapped in the MLI turns to ice. The pumpdown is drastically limited by the ice's sublimation rate. An air purge adds heat to the water where it can again be pumped as water vapor. It was found that there is little benefit in backfilling with dry nitrogen on the initial purge.

Following the pump down of the cryostats by mobile roots blowers, vacuum is maintained with turbomolecular pump stations. Three turbopumps are located near the endpoints (Q4) and midpoint (Q21) of each long arc cryostat. Mobile turbomolecular pump stations are installed on interconnect pumpout ports nearest any identified leaks to maintain satisfactory insulating vacuum. These mobile pumps are tapped into the overhead RS-485 network and operated in like manner to the permanent turbos.

A network of pumpout ports and transverse conduits, designed and implemented by Welch[3], was added to address the presence of He in the insulating vacuum. Transverse conduits, located at each magnet interconnect, are high vacuum conductance paths linking the three cryostat regions. Pumpout ports are also located at each interconnect. The pumpout ports and transverse conduits were added to insure two conditions. First, that in the event of an internal helium leak, they would create a helium pressure gradient with sufficient resolution to allow locating the leak to within one interconnect. Second, they provide adequate conductance to ensure that leaks of substantial size could be effectively pumped by a turbomolecular pump (TMP) station.

The conductance of the transverse conduit and pump speed of the pump station were sized with the geometry of the arc cryostat in mind. Preliminary estimates on the required conductance of the conduits and pump speed were based on a voltage analogue (resistor network) of the magnet string. A room temperature resolution of 12% across a CQS magnet was observed during testing of Full Cell 2. To increase resolution, and pump leaks more effectively, the conductance of the conduit was improved to ~400 l/s for final design. This yielded an effective He pumping speed of ~110 liters/sec in the innermost region of the transverse conduit with a 150 l/s turbopump mounted at that interconnect. This effective speed allows a 10^{-2} Torrl/s helium leak to be pumped while maintaining satisfactory insulating vacuum.

A Balzers TPH 180H turbopump with a high He compression ratio of 10^5 was selected which insures helium removal from the cryostat. The high turbopump compression ratio coupled with operating modes of the pump station relaxes backing pump sizing requirements. A small backing pump (Balzers UNO 1.5) costs less, has lower operating costs, and fits in a smaller envelope.

Several ancillary features of the pump station include a foreline isolation valve, high vacuum and foreline vent valves, leak check port with manual valve and a foreline gauge port. The pump station is mounted to an electropneumatic valve that isolates the pump station from the cryostat. Gauge ports on either side of the valve seat add to the control system feed back and system diagnostics capability. A schematic of the pump station is shown in Figure 2. A single board computer with FLASH PROMs was used to integrate the gauge controller, TMP power supply, and I/O board. A Custom C+ program compiled and downloaded to the controller memory also adds flexibility to station operation.

Cold-Bore Vacuum System

All UHV components for the cold bore system utilize ConFlat® type flanges, and were baked at $\geq 250°C$ and leak checked to $< 1 \times 10^{-11}$ Atm cc/sec helium prior to installation. The beam pipes of each magnet were joined at each interconnect region with an RF shielded bellows. Beam profile monitors (BPMs) are located at every other interconnect. Activated charcoal sorption pumps and gauge conduits are located in an alternating fashion at non-BPM interconnects.

The cold bore was roughed down with a molecular sieve sorption pump to a few microns. Special care was taken to *throttle* the roughing valve so charcoal would not be drawn from the sorption pumps into the cold bore. Turbopumps were used to lower the pressure to $\sim 10^{-5}$ Torr (at the pump). All flanges and welds were checked using an ultra-sensitive leak detector to a sensitivity of 1×10^{-11} Atm-cc/sec He. The turbopump was subsequently valved off and the pressure was allowed to creep up to $\sim 10^{-2}$ Torr before the cooldown. After the cooldown, the cold cathode gauges in the yellow arc read from mid 10^{-10} to low 10^{-9} Torr levels. These readings were due to the localized outgassing of the gauge conduits and the ambient instrument trees where the gauges are installed.

The cold cathode gauges used for the UHV cold bore contained low activity Am^{241} sources to aid gauge discharge startup.[4] No delays in gauge startup were noted. Gauge pressure readings for all installed gauges were logged for the duration of the test.

Warm-Bore Vacuum System

All UHV components for the warm bore system utilize ConFlat® type flanges, were baked at ≥250°C and leak checked to $<1\times10^{-11}$ Atm cc/sec helium prior to installation. There were no problems associated with the installation of any warm bore hardware. All beam tube and beamline components were surveyed. The warm bore systems were roughed down and the sputter ion pumps were turned on. The warm bore systems received neither a bakeout nor a titanium sublimation pump (TSP) flash. A pressure of 10^{-9} Torr was attained in all warm-bore sections. In addition, one standing wave cavity (storage cavity) was satisfactorily conditioned into the sputter ion pumps (Figure 3). Finally, an all-metal RF-shielded gate valve, located at Q3, was successfully baked at 275°C. This test was done with the magnet string at cryogenic temperature with no adverse heat load through the warm to cold transition.

Instrumentation & Control System

Controls

The backbone of the RHIC vacuum instrumentation system consists of a network of distributed programmable logic controllers (PLCs). Figure 4 depicts the vacuum instrumentation and control (I&C) system architecture. All gauging, ion pumps and sector valves were interfaced with the PLC systems. Each PLC was outfitted with a complement of 24 Vdc input and output (I/O) modules and serial communication modules. Inputs were generated by gauge controller relay contacts and sector valve limit switches. The PLC generated 24 Vdc outputs for the valve solenoids and beam permit links. In addition, the PLC supplied the central Controls System front end computer (FEC) with the vacuum instrumentation status and readings. A relatively simple spreadsheet format was used to display the collected data on vacuum system parameter editing tool (PET) pages, viewable from many remote terminals distributed throughout the RHIC complex. A single man-machine interface (MMI) provided the means of viewing the status of the vacuum system beam permit and all sector valves in use for the sextant test, and the means to control the state of those valves via the PLC multi-drop network. The MMI resides in a 486-based personal computer at the 1006B service building.

Gauging

For the first sextant, a total of seventy cold cathode gauges (CCGs) and twenty-three thermocouple gauges (TCGs) were used to monitor the vacuum in the insulating and beam tube volumes and provided interlocks for valve control and beam permits. A portion of the instrumentation distribution is shown in Figure 5. The cold cathode gauges were inverted magnetron type gauges with an operational range from 10^{-11} and 10^{-3} Torr. The TCGs used were convection-enhanced Pirani type gauges with an operational range from 1×10^{-3} to 1000 Torr. All warm bore, cold bore, and insulating cryostat vacuum systems used the same high vacuum and low vacuum gauges. All the gauges are bakeable, and the warm bore and cold bore CCGs are outfitted with Am^{241} sources to facilitate ignition at low pressures to avoid possible long start time delays.

Fifty gauge controllers capable of operating two CCGs and two TCGs were distributed along two RS-485 serial communication networks. Pressure data was transmitted from all gauge controllers through the RS-485 bus to the PLCs located up to 2,200 feet away. The readings were then transferred to the FEC and made available for viewing in table and graphical forms at remote terminals. An analog signal from a CCG on the storage cavity was used to interlock the RF power supply during conditioning. There were no gauge controller failures.

Ion Pump Controllers

Twelve ion pumps installed in several warm bore regions were operated remotely from the service buildings for the FST. Pressure, voltage and current readings were gathered from the ion pump controllers (IPCs) through an RS-485 network (separate from the gauge controllers) and similarly made available for viewing at remote terminals. Several IPCs failed during the test due to high-voltage termination complications. Most ion pumps sustained indicated pressures in the 10^{-9} Torr range.

Partial Pressure Analyzers

Data was collected from eight partial pressure analyzers (PPAs) distributed along the yellow arc and triplet cryostats. The vacuum in the blue arc was not good enough for PPA operation ($< 1 \times 10^{-4}$ Torr). A stand-alone personal computer (PC), located in the 1006B service building, was used to take daily analog scans, and to log helium and nitrogen pressure trends upon introduction of leaks and during cryostat temperature cycling. This Windows® based software, supplied by the vendor was not flexible enough for the type of data logging required, and produced volumes of data that required significant manipulation to be useful. Software similar to that developed for reading the gauges and ion pumps will be generated for ring operation. The PPA data clearly showed peaks for air in the cryostats with air leaks and helium peaks in those with helium leaks. Water outgassing from the multi-layer insulation could be seen decreasing in magnitude over time as the water was pumped by the coldmass. In addition, mass 3 peaks were recorded while HD was being introduced during a sector 4 triplet leak check.

Uninterruptable Power Supplies

Uninterruptable power supplies (UPS), installed in the service building racks, insure that short power interruptions would not cycle the all-metal sector valves needlessly. Equipment that had the capability of triggering sector valve closures in the event of a loss of power was backed by a UPS, including the two PLCs and all gauge controllers in the service buildings.

III. LOCATING HELIUM LEAKS WITHIN THE CRYOSTATS

Identification of leaks

Once the insulating vacuum on the cryostats was established, large internal helium leaks were observed in both the 4:00 and 5:00 triplets. These leaks manifested themselves as higher than normal helium background levels with ~1 Atm of helium on the internal process lines. A subsequent leak check revealed internal leaks in the blue and yellow long cryostats as well. A

series of pressure tests were conducted to isolate the leaks to specific process lines in all of the vacuum envelopes. Each line was individually pressurized to 15 atm while maintaining vacuum on the other lines. To expedite completion of FST, a priority of locating and repairing all yellow circuit leaks, as well as the blue heat shield, was established. Table 1 shows a summary of the known leaks and their room temperature size and locations.

The above mentioned pressure tests were done at a reduced sensitivity due to a high total pressure (typical for large system leak checking) of $\sim 10^{-2}$ Torr on average. Because the leak detector was sampling 10^{-4} to 10^{-3} of the signal, the actual leak rate was estimated to be proportionately higher than that indicated on the leak rate meter. For example, the blue return line in the 5:00 triplet had an indicated leak of $> 1 \times 10^{-6}$ atm cc/sec air eq. The actual leak rate was $> 10^{-3}$. This implies that, at the available sensitivity, any leak(s) $\leq 10^{-5}$ atm cc/sec air eq would go undetected. Internal leaks were quantified by throttling and desensitizing a Veeco MS-17 leak detector connected to the foreline of a turbopump. A 10^{-5} atm cc/sec air eq calibrated leak was mounted in the turbo foreline upstream of the leak detector. The turbo forepump was used to help reduce the helium pressure entering the leak detector. The helium entering the leak detector was further reduced by using a Varian® variable leak until the indicated leak rate was 1/1000 that of the 10^{-5} leak. This enabled measurements of leaks as large as 10^{-2} atm cc/sec.

Once the cryostats were opened, short of special fixtures, the only tool available for locating leaks was sniffing while pressurizing the lines to 15 atm. This approach can only detect 10^{-5} leaks, when parked on the leak. Bagging and accumulating helps identify 10^{-5} leaks, but provides little benefit for locating smaller leaks. To highlight this example, a yellow utility leak of $\sim 10^{-5}$ was located by leaving the line under 80 psig for 72 hours with the cryostat at atmospheric pressure. This yielded a slight increase in background of $\sim 3 \times 10^{-9}$ with a sniffer probe. A leak of $\sim 10^{-6}$ would require an impractical 720 hours, or 30 days, of accumulation to be observed with the leak detector. When cold, the leak was quantified at $\sim 10^{-2}$, and was found to be the upper limit for maintaining a satisfactory insulating vacuum of $\sim 10^{-4}$ Torr.

One serious obstacle in identifying leaks was the problem of helium blow-by at the cryogenic valve boxes. During the high pressure 15 atm testing, the valve seat was lifted causing helium to bleed into other leaking lines. This leakage was not high enough to be observed by cryogenic pressure gauges, but significant enough to cause false readings. Measures were taken to ensure the valves remained on their seats. A problem of a more subtle nature occurred when leak checking the blue arc. By pressurizing individual lines, it was believed that a large leak existed in the magnet line, with smaller leaks in the utility and supply line. Using gradients and sniffers, it appeared that all the leaks were located within one interconnect of each other. After repairing the large magnet leak, the utility and supply leaks could not be reverified. It was determined a leak existed in the magnet recooler(s), allowing helium from the supply line into the magnet line during leak checking.

Locating Leaks Through The Use of Helium Pressure Gradients

Arc Cryostats

After identifying which process lines leaked and quantifying the size, knowing which interconnect to cut open had to be determined. This was accomplished by measuring the established longitudinal helium pressure gradient. Each interconnect was sampled through a Varian® variable leak. Once set, the variable leak was not adjusted during the gradient measurements. The calibration of the Veeco MS-17 leak detector had to be checked at each interconnect and the time of sampling had to be consistent. A room temperature 10^{-3} atm cc/sec air eq. yellow arc utility line leak was located by the gradient shown in Figure 6. The graph showed a clear high point at interconnect YO4D13-Q14. Upon opening the interconnect, the leak was found to be at a repaired weld seem at the recooler end of the rush line. This particular joint was difficult to weld due to the geometry of the recooler magnet. It should be noted that there was an additional utility leak two orders of magnitude smaller at magnet YO5D13. It was masked by the larger utility leak and was not found until the larger leak was fixed. This was the first arc gradient taken and subsequent gradients yielded less desirable results. Resolution of 3-6% across a CQS and 8-15% across a dipole were typical when measuring gradients. As a result, great care in partial pressure measurements had to be taken. Improvements in resolution can be made by bracketing the leak more closely with turbopumps. Subsequent to the repair of the first utility leak, a gradient revealed a second leak in the utility line. The leak size was determined to be cryogenically acceptable and as a result gradients were taken with the magnet string at 4.4°K (Figure 7). Consequently, the leak size increased to 1.5×10^{-2} atm cc/sec air eq. Based on the results of the gradients, an additional turbopump was placed at interconnect YO5Q14-D13. This reduced the total pressure at this interconnect from $\sim 10^{-3}$ Torr to $\sim 10^{-4}$ Torr. With the mobile turbo valved out and the local pressure at $\sim 10^{-3}$ Torr, no adverse heat load was placed on the magnets. However, single leaks of this size should be considered an upper limit for the insulating vacuum system.

The data shown in Figure 7 does not clearly indicate which interconnect to cut open. Based on the location of the previous leak, the decision was made to open interconnect YO5Q14-D13. While no leak was found at the interconnect, a higher than normal helium background was found within the D13 dipole cryostat. The dipole's other interconnect (YO5D14-Q13) was opened and using a sniffer, the leak was found to be within the D13 dipole magnet. The utility rush lines were cut and the dipole's utility line was isolated and vacuum leak checked. The most probable location is the pipe anchor weld near the middle of the cryostat.

Triplets

Triplet geometry impacts the ability to locate internal leaks with the use of helium pressure gradients. The triplet cryostats provide insulating vacuum for magnets in both rings, requiring a significantly larger diameter vessel. The larger diameter cryostat results in relatively high longitudinal conductances which reduce the effectiveness of the transverse conduits in establishing a pressure gradient. As a result, it proved more difficult to locate leaks within the triplets. In most cases, the gradients were taken before the system equilibrated. This was done to gain an

advantage by sampling while the gradient was most pronounced, but resulted in difficulty interpreting the data due to the helium pressure rising during sampling. Letting the system equilibrate first may have yielded sufficient resolution across the magnets, and yielded clearer results. In the case of the 5:00 triplet, the gradient data yielded inconclusive results, and probing with a sniffer was relied on as the primary diagnostic tool. An internal baffle intended to reduce longitudinal conductance was installed at the DO-Q1 interconnect in the 4:00 triplet. Due to insufficient data, conclusions as to the effectiveness of the baffle could not be reached.

With the system bled up to atmosphere, each interconnect was drilled and probed with a sniffer to either confirm or reject the gradient data prior to interconnect cutting. Once the interconnect was cut open, a sniffer was used to locate the leaks. The majority of the leaks found were due to either damage from the ultrasonic welder, or corrosion in the weld seam of the heat-shield flex line bellows.

Contrived Leak

A contrived leak was introduced 50 meters from YO5D13 at interconnect YO5Q17-D16 into the 300°K region of the cryostat while at 4.4°K. The leak was set to $2x10^{-3}$ atm cc/sec air eq and subsequently increased to $2x10^{-2}$ atm cc/sec air eq. The results are shown in Figure 8. It can be seen that the $2x10^{-3}$ leak is masked by the larger $1.5x10^{-2}$ D13 utility leak. The contrived leak was then increased to $2x10^{-2}$, roughly the same size as the D13 leak. The gradient showed that the contrived leak was visible and slightly (25%) higher than the existing D13 leak. This was due to the contrived leak being introduced at the 300°K region, while the D13 leak was located at the 4.4°K region. However, this test showed that differentiating leaks of similar size (<2x) within ~50 meters from each other is difficult.

IV. HELIUM PUMPING USING ACTIVATED CHARCOAL

Since the coldmass has a limited capacity for pumping helium, unmitigated helium leaks would increase cryostat pressure and eventually the heat load beyond tolerable limits of the refrigeration system. As described earlier, turbomolecular pump stations are employed in the presence of helium leaks to extend the machine duty cycle. The original requirements for subsystem and equipment specification was based on continuous machine operation with no planned shutdown. TMP stations have no fixed capacity, are accessible for maintenance and repair, and are therefore suited to the original doctrine. However, the duty cycle of the machine will not be continuous, and regular and periodic down time is planned. This periodic downtime which includes a refrigerator shutdown and warm-up of the machine might provide additional options for contending with insulating vacuum helium leaks, and possibly reduce the quantity of permanently installed TMP stations.

This pumping strategy would only be pursued in the shorter cryostats for two reasons. First, leaks in longer cryostats are easier to find and pump. Without the foresight to know

precisely which interconnects might have leaks, all magnets would require a charcoal patch. Second, the charcoal needs to be exposed to vacuum for a long period of time at room or elevated temperature to be conditioned for helium cryosorbing. This is unlikely to be an option for long cryostats, but can probably be arranged for the shorter cryostats. To insure future cryosorbing capacity subsequent to pumping on helium leaks, warm-ups would require placement of a turbopump near the leak to most effectively remove the helium from the cryostat. With charcoal located at each interconnect and the possibility of many leaks, the possible benefit of reducing TMP stations is lost. The simplest approach for mitigating helium leaks on the arc cryostats therefore remains to be TMP stations.

RHIC Full Cell 2 tests verified that the coldmass has significant helium pumping capacity. Prior to warm up of Full Cell 2, a total quantity of 250 Torr·*l* was injected into the cryostat. Had this introduction of helium been at room temperature, it would have driven the cryostat pressure to $3x10^{-2}$. However, due to cryogenic temperatures, the resultant pressure was a factor of 10 lower and dropping. If one looks at the adsorption isotherm for stainless steel, the predicted capacity of the cold piping at 10^{-2} Torr is only ~40 Torr·*l*. This is based on the extrapolation of isotherm data presented by Wallen.[5] It is believed that the additional capacity that was observed stemmed from diffusion into the inner cold MLI layers where isotherms formed on the cold MLI jacket in close proximity with the 4.4°K cold surfaces. It was also observed that the cryopumping speed of the cryogenic surfaces was high. During the last phase of Full Cell 2 testing, prior to warm up, gas was introduced at a rate of ~$5x10^{-2}$ Torr·*l*/s. The pumping speed of the cold surfaces due to helium thermalization maintained cryostat pressure at $7x10^{-4}$ Torr, suggesting a cryopumping speed comparable in size. It should also be noted that this final introduction did not create a measurable heat load on the cryogenic system. However, as is discussed later, throughputs of this size would quickly saturate the cryostat if not pumped. In all cases subsequent to introduction, a slow pressure decay was observed. This can be seen in Figure 9.

The cold surfaces for Full Cell 2 included both the magnet string and supply line. In intimate contact with these cold surfaces is a MLI blanket comprising sixteen layers of DAM with two layers of Reemay spacer per layer of DAM. The expected temperature gradient across this blanket varies in linear fashion from 4.4°to ~12°K.[6] Assuming the isotherm for helium on the aluminized material is that of stainless steel at 4.4°K, and varies as a function of temperature similar to that of activated charcoal (i.e. surface capacity at 4.4°K is 10x that at 15°K), the capacity for each layer can be approximated. The total theoretical capacity for Full Cell 2 would be roughly 800 Torr·*l*. It should be noted that the capacity of the MLI is based on theoretical equilibrium conditions. Conductance limitations to the inner layers could reduce the effective capacity. A predicted capacity half the theoretical value of 32 Torr·*l*/meter cryostat was chosen as a conservative value.

The two cryostats installed with charcoal panels were the yellow injection region cryostats, namely YO5DU3-YO5Q7 and YO5Q8-YO5Q9. Each cryostat received two panels. Each panel contained ~23 grams of charcoal and had a surface area of 230 cm^2. A panel was placed around the BPMs at each end. An internal leak between the cold bore and insulating vacuum in the YO5DU3-YO5Q7 rendered it useless for testing. The YO5Q8-YO5Q9 had no leaks and maintained a vacuum of 1×10^{-5} Torr for approximately two weeks prior to cooldown. This provided ample time to condition the charcoal. For these reasons, and limited resources, helium capacity was only tested on the YO5Q8-YO5Q9 cryostat.

The density of the charcoal is ~0.1 grams/cm^2. Assuming ideal thermal contact with the 4.4°K cold mass results in a panel temperature equaling the cold mass, the expected speed would be ~4 l/s cm^2, with a capacity of ~10 Torr·*l*/cm^2.[7] For the combined two panels, this yields a speed of 1840 l/s with a capacity of 4600 Torr·*l*.

The test apparatus consisted of a NIST traceable known volume with capacitance manometer as a helium source, a PPA to verify gas purity, and a standard complement of insulating vacuum gauges (a TC and CCG pair), and additional gauges at the opposite end of the cryostat. Over the course of two weeks after beam tests, a total of 300 Torr·*l* of helium was added to the cryostat volume. With an estimated cryostat volume of approximately 5120 liters, the quantity of gas added was confirmed during warm-up when a cryostat pressure of 60 microns was measured at room temperature. No measurable heat load was placed on the cryogenic system during the test.

Initially, helium was added slowly at a rate of approximately one Torr·*l*/min. This rate was increased once it was apparent that the cryostat pressure was less sensitive to the addition of helium. This is best illustrated in Figure 9 which shows cryostat pressure as a function of time and introduced helium. Most evident in this graph is the ability of the cold surfaces to accept large amounts of helium introduced over relatively short periods of time. To further illustrate this, Full Cell 2 data and FST test data where plotted similarly in Figure 10. It should be noted that cryostat volumes and cold surface areas differed for Full Cell 2. Estimates of the A_{cold}/Vol ratio differs by a factor of two. The helium in Full Cell 2 was introduced to the innermost 4.3°K region through a capillary. Helium introduced during FST test was done at the 293°K region. A comparison of the two curves show similar pressure decay slopes subsequent to helium introduction. There was no observable improvement in cryopumping speed due to the presence of the charcoal.

The helium capacity for both Full Cell 2 and FST is shown in Figure 11. The cold pressures were plotted against room temperature pressures to illustrate the effectiveness of the cold surfaces. FST data shows a reduction in helium pressure over Full Cell 2. It should be noted that, due to time constraints, the introduction of the final ~200 Torr·*l* was over a 90 minute period for Full Cell 2. Helium was bled in over a much longer duration in FST (Figure 9), allowing the system to equilibrate after each introduction. This makes direct comparison difficult. Based on theoretical isotherms, insufficient quantities of helium were introduced to saturate the cold surfaces

during FST and measure the capacity of the charcoal panels.

By using the theoretical capacity of the charcoal, estimates of operational time were calculated. Because the cold surfaces and charcoal have such a high pumping speed, the limiting factor for extending operation is the capacity. Figure 12 shows the expected operational time of a 20 meter cryostat with and without the use of charcoal. This is based on normal operation where magnets, supply and utility lines are cold (unit capacity of 16 Torr·*l*/meter without charcoal). For example, the short YO5Q8-YO5Q9 cryostat (~20 meters long, 320 Torr·*l* capacity) could tolerate a 10^{-2} atm cc/sec He leak for a maximum of 400 hours (16 days). The use of charcoal would increase operating time to 6400 hours (266 days).

V. HELIUM WAVE PROPAGATION WITHIN THE COLD BORE BEAM TUBE

In RHIC first sextant test, the He propagation in cold bore at 4.4 K was measured over a 12-day period. Helium was bled into the cold bore using a calibrated He leak of $3X10^{-5}$ Torr·*l*/s (20 C). The equivalent He leak rate at 4.4 K is proportional to the temperature and is $4.5X10^{-7}$ Torr·*l*/s. The leak was introduced through the all-metal valve mounted on the YO4-PC12 instrument tree. The locations of the CCGs and the sorption pumps in both directions and their distance in meters from the leak are shown in Figure 13. The CCG readings were continuously monitored and recorded by the RHIC data logging system during the measurements. Typical plots of the logged CCG readings during the measurement are shown in Figure 14 for those toward 4:00 and in Figure 15 for those toward 5:00. The changes in CCG readings were divided by 1.2 to obtain the true cold bore He pressure at 4.4 K.

Two measurements were conducted in the 12-day period. In the first run, helium was bled in for four hours then valved off for three days. The amount of He bled-in over this 4-hour period is approximately 0.0065 Torr·*l*. In the second measurement, helium was continuously bled in for 9 days before being valved off with approximately 0.35 Torr·*l* He bled in. The CCG readings increased sharply when the He fronts reached the particular gauge locations, then leveled off over the whole nine day period. The time for the first observable sign of the pressure increase and the time for the readings reaching plateau at the CCGs are listed in Table 2 together with the plateau CCG readings and the corrected He pressure in the cold bore. The He front traveled slower toward 4:00 than toward 5:00. The sorption pumps toward 4:00 are positioned closer to the leak than those toward 5:00, which reduced the quantitiy of He progressing down the tube.

In a long cryogenically cooled tube, helium will initially have a limited propagation speed due to the physical adsorption of He on the surface. Hobson and Welch[8] developed a model based on steep adsorption front and equilibrium adsorption isotherm to describe the phenomenon. The model assumes that helium is initially strongly adsorbed by a narrow band of the cold bore wall at the leak. With the buildup of He on the surface, the adsorption-desorption process will reach an equilibrium and becomes that of the adsorption isotherm. Only then the leading edge of the pressure zone can progress down the tube and adsorbed by the 'fresh' band of the cold bore or

pumped by the sorption pump when the foot of the adsorbed layer reaches the pump. The pressure at the He front is given by $P(x) = Q/ Ca$ with Ca the aperture conductance of the cold bore = $0.91\pi D^2 (T/M)^{0.5}$ = 142 l/s for He at 4.4 K, and D the diameter of the pipe. The pressure at the leak is given by $P(0) = Q/Co$ with $Co = Ca / (1+0.75 x / D)$ and x the location of the He front. Therefore the pressure at the leak and at the He fronts can be calculated for the selected x.

The other important assumption of the model is that the pressure profile is a linear function of x between the leak and the front, since the He flow is constant between them. With the known pressure at the leak and at the front, the pressure profile in each segment then can be calculated without reference to adsorption isotherm or time. The next step is to integrate the total amount of He which entered the cold bore. The amount of He adsorbed σ at any point x is given by the DRK adsorption isotherm equation[10] $\ln (\sigma / \sigma_m) = - B (RT \ln P(x) / \ln Po)$ where σ_m is the monolayer coverage, R = 1.986 cal/mol deg, Po = 900 Torr the saturated vapor pressure of He at 4.4 K. Values of 1.27×10^{15} atoms/cm^2 for σ_m and 5.48×10^{-5} mol^2 cal^{-2} for B, the empirical constants as recently reported for stainless steel,[5] are adopted in our calculation. Using the adsorption isotherm and the known pressure profile, the quantity adsorbed by the cold bore before passing the first sorption pump is obtained, so is the time to reach that pump by dividing the quantity entered with the leak rate. Using the same approach and including the successive pumps, the pressure profile, the quantity adsorbed by the cold bore, the amount pumped by the sorption pumps and the travel time of the He front can then be calculated. The pressure and the arrival time at any location, such as at the CCGs, can be derived for different value of x.

The calculated travel time for the He pressure front is plotted together with the measured travel time (time with initial pressure rise and time with plateau reading at the CCGs) in Figure 16 versus the distance from the leak. Negative values in distance are those toward 5:00. The knees on the calculated curves give the locations of the sorption pumps. Toward 4:00, the pressure increases were very steep and the initial arrival time and the plateau time were both within 40% of the calculated ones. Toward 5:00, the measured travel times are shorter than the calculated ones by as much as one decade, if only considering the initial pressure rise time. As shown in Figures 14 and 15, the pressure increases toward 5:00 were also not as steep as compared with those toward 4:00. No apparent cause can be attributed to this unexpected observation toward 5:00.

The cold bore He pressures derived from the changes in the plateau CCG readings are also listed in Table 2 and plotted versus the distance in Figure 17 together with the calculated pressures at time ~6 days. Again, the knees on the calculated curves give the locations of the sorption pumps. The measured cold bore pressures are in reasonable agreement with the calculated ones in both directions. This result also validates the need and the effectiveness of the sorption pumps in slowing the speed of the He front and in reducing the magnitude of the He pressure zone. In a similar study[9] with a leak of 1×10^{-6} Torr·*l*/s (4.25 K) and without pumps, the magnitude of the He pressure at x = 75 m was found to be two decades higher and the arrival time one-tenth of those of the present study.

Table 2. Measured arrival time and pressure at the cold cathode gauge locations

CCG Name	Distance to Leak(m)	Initial Arrival Time(hr)	Plateau Arrival Time(hr)	CCG Reading* (Torr, 20 C)	Cold Bore He P** (Torr, 4.4 K)
PC6	85	120		8.5×10^{-10}	1.25×10^{-10}
PC7	75	62	81.75	3×10^{-9}	1.75×10^{-9}
PC9	45	8.5	19.75	1.6×10^{-8}	1.12×10^{-8}
PC10	30	4.5	8.25	2.1×10^{-8}	1.74×10^{-8}
PC14	30	2.3	7.75	1.4×10^{-8}	1.08×10^{-8}
PC16	59	8	23.75	9×10^{-9}	6.5×10^{-9}
PC18	89	13.25	32.75	3×10^{-9}	1.17×10^{-9}
PC20	119	30.75		1.7×10^{-9}	2.5×10^{-10}

* flattened readings after the initial steep rise at 20 C
**derived from the CCG reading subtracted by the background reading(before He leak was introduced) and then divided by 1.2 for thermal transpiration and the gauge sensitivity for He

VI. CONCLUSIONS

Insulating Vacuum

Due to an insufficient quantity of blower stations, turbopump stations were used to help maintain rough vacuum levels (roughly 10-100 microns) prior to cooldown and to generate pressure profiles for leak testing. The combination of transverse conduits and pump stations proved adequate for leak checking the long arcs. However, since the roughing mode was not intended during the design of the pump station, the backing pump was less than adequate for the high water vapor load associated with this room temperature operating mode manifested in frequent oil changes. In the worst case, pump stations would shut down due to high foreline pressures.

The plan to improve pump station performance to satisfy this roughing mode will be accomplished by improving the foreline conductance (KF16 to KF25 components) and by changing to a larger mechanical pump (two stage 10 cfm rotary vane pump). Once the machine is cooled to operating temperatures, the pump station's only function is to pump on helium leaks. Pump stations proved to be effective in this capacity. The larger mechanical pumps required for roughing are not necessary for this low throughput function. Therefore, only a portion of the pump stations will be outfitted with the larger forepump and foreline. One modified pump station will be placed at the midpoint (Q21) of each arc cryostat, and on each triplet/DX cryostat. The remaining unmodified pumps will be used for pressure profile generation and helium leak pumping during operation.

Instrumentation & Control System

Changes in the cryostat instrumentation layout will be instituted for the remaining sectors based on FST results. TMP stations, originally placed at the end points (Q4) and midpoint (Q21) of the arcs will be placed at Q10, Q21, and Q10, to increase pressure gradients for better resolution during leak testing. Gauges will be situated at Q4, Q14, Q21, Q14 and Q4 to better monitor pumpdown. The gauges at Q21 will be tied into the TMP gauge controller. Partial pressure analyzer (PPAs) will be located at Q6, Q14, Q21, Q14, and Q6. These changes will provide a better distribution of gauging in the remaining five arcs.

The vacuum system PLCs were reliable and stable for the duration of the test, as was the MMI. Gauge pressure readings displayed by the FEC suffered intermittent glitches, where the readings took on impossible values. These relatively infrequent erroneous readings did not impact the PLC valve interlock or beam permit integrity, only the data acquisition performed by the FEC. Sporadic disruptions occurred in the PLC-to-FEC communication causing periods of lost data. Since the test, the cause of the communication problems has been identified and resolved. The use of two-way radios in close proximity to the gauge controllers caused detrimental interference (artificial pressure spikes) which caused pressure interlocks to close sector valves.

Locating Helium Leaks Within the Cryostats

The transverse conduits provided the necessary resolution to locate leak(s) within one interconnect using the permanent turbos. Resolution can be improved by locating turbos closer to the leak. Leaks of similar size in close proximity to each other proved difficult to differentiate. It was shown that a large leak can mask a smaller one, even when separated by considerable distance. Because no benefit in longitudinal resolution could be seen across the vacuum baffle in the 4:00 triplet, no baffles will be used in the remaining triplets.

Helium Pumping Using Activated Charcoal

Insufficient quantities of helium were added to the FST cryostat to adequately test the capacity of the charcoal panels. The presence of the charcoal does not noticeably improve the already considerable cryosorption speed of the cold surfaces. With the installation of the panels in the short cryostats, a given leak can be tolerated roughly ten times longer.

Helium Wave Propagation Within the Cold Bore Beam Tube

The propagation of the helium leak in the cold bore at 4.4 K has been measured over a 12-day period. Using the steep adsorption isotherm model developed by Hobson and Welch,[8] the travel time and the pressure profile in our cold beam pipes have been calculated and compared favorably with the measured values. The model can be used to estimate, with reasonable accuracy, the impact of He leaks into the cold bore. The effectiveness of the sorption pumps in slowing down the traveling of the helium fronts and in reducing the magnitude of the He pressure zone has been verified.

Acknowledgments:

The authors would like to thank David Loughlin, Charles De La Parra, Paul Mickaliger and Douglas Zigrosser for their exceptional efforts during the FST commissioning. Thanks also to Michael Iarocci and his staff for cryogenic support during leak checking.

References:

[1] R.J.Todd, D.J. Pate, K.M. Welch, "Outgassing Rate of Reemay Spunbonded Polyester and Dupont Double Aluminized Mylar", RHIC Technical Note BNL-49345, August 1993.

[2] R.J.Todd, D.J. Pate, K.M. Welch, "Modeling of RHIC Insulating Vacuum for System Pumpdown Characteristics", RHIC Technical Note BNL-49181, June 1993.

[3] K.M.Welch, RHIC Design Manual, Brookhaven National Laboratory, August 1992.

[4] K.M. Welch, L.A. Smart, R.J. Todd, J. Vac. Sci. Technol., A14, 1288 (1996).

[5] E. Wallen, J. Vac. Sci. Technol., A15, 265(1997).

[6] G.E. McIntosh, "Layer by Layer MLI Calculation Using a Separated Mode Equation", Advances in Cryogenic Engineering Vol. 39, part B, (Plenum Press, New York).

[7] H.C. Hseuh, T.S. Chou, Worwetz H.A., Halama H.J., "Cryosorption Pumping of He by Charcoal and a Compound Cryopump Design for TSTA", IEEE CH1441-5/79/0000-1568.

[8] J.P. Hobson and K.M. Welch, J. Vac. Sc.. Technol., A11, 1566 (1993)

[9] E. Wallen, J. Vac. Sci. Technol., A15 (1997) (in press).

[10] P.A. Redhead, J.P. Hobson and E.V. Kornelson, the Physical Basis of Ultrahigh Vacuum (Chapman and Hall, London, 1968), p 46.

Figure 1. Pumpdown of 13 Magnet String (7 Dipoles, 6 CQS)

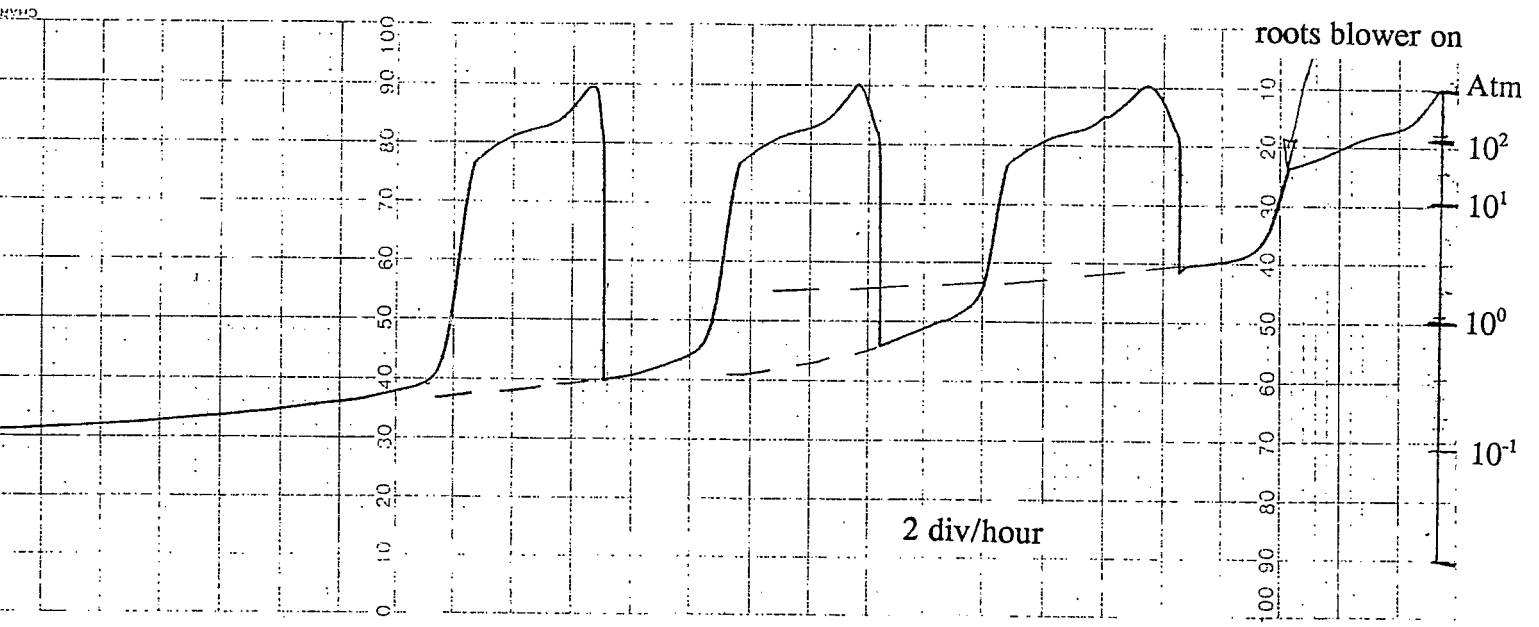

Table 1. Summary of Internal Leaks Within FST Vacuum Envelopes

VACUUM ENVELOPE	HEAT SHIELD		SUPPLY		RETURN		UTILITY		MAGNET	
	size	location	size	location	size	location	size	location	size	location
5:00 TRIP BLUE					>10E-6	5			~1 std cc/s	9
5:00 TRIP YELLOW	~1E-4 std cc/s	1							~1 std cc/s	10
									~2E-3 std cc/s	14
DU3-Q7										
Q7-Q8										
ARC YELLOW							~1E-3 std cc/s	7		
							~1E-5 std cc/s	15		
ARC BLUE									~1 std cc/s	11
4:00 TRIP BLUE	~1E-4 std cc/s	2	~1E-3 std cc/s	4			>1E-8	8	>1E-7	12
4:00 TRIP YELLOW	~1E-4 std cc/s	3			~1 std cc/s	6			~1E-4 std cc/s	13

location:

1 two leaks located along weld seam of flex line at the Q3-VJR interface.
2 one leak found in weld seam of bellows at the mid point of flex line at the Q3-VJR interface.
3 one leak found in weld seam of bellows ~8" down from the VJR-Q3 interface.
4 one leak found in bellows ~8-12" down from VJR-Q3 interface.
5 ?
6 one leak foundin bellows ~8" left of Q3-VJR interface.
7 one leak found at O4D13-Q14 interconnect on D13 end of utility pipe. leaked where automatic weld had been repaired by hand.
8 ?
9 minimum of two leaks located in bellows of power lead flex line at Q1-Q2 interface. both leaks above the heat shield.
10 two leaks located in bellows of power lead flex line at Q1-Q2 interface. one leak above heat shield, the other below. one leak located in bellows of main flex line at Q3-VJR interface. leaked at the mid point of flex line.
11 Q7-DU7 upper bellows roll flange (DU7 end)
12 ?
13 one leak located in bellows of power lead flex line at Q2-Q3 interface. leak was above the heat shield.
14 Q1-Q2 power lead flex line
15 within D13 dipole (suspect pipe anchor weld)

r.todd "fstf.wk4"

Figure 2. RHIC TMP Station Schematic

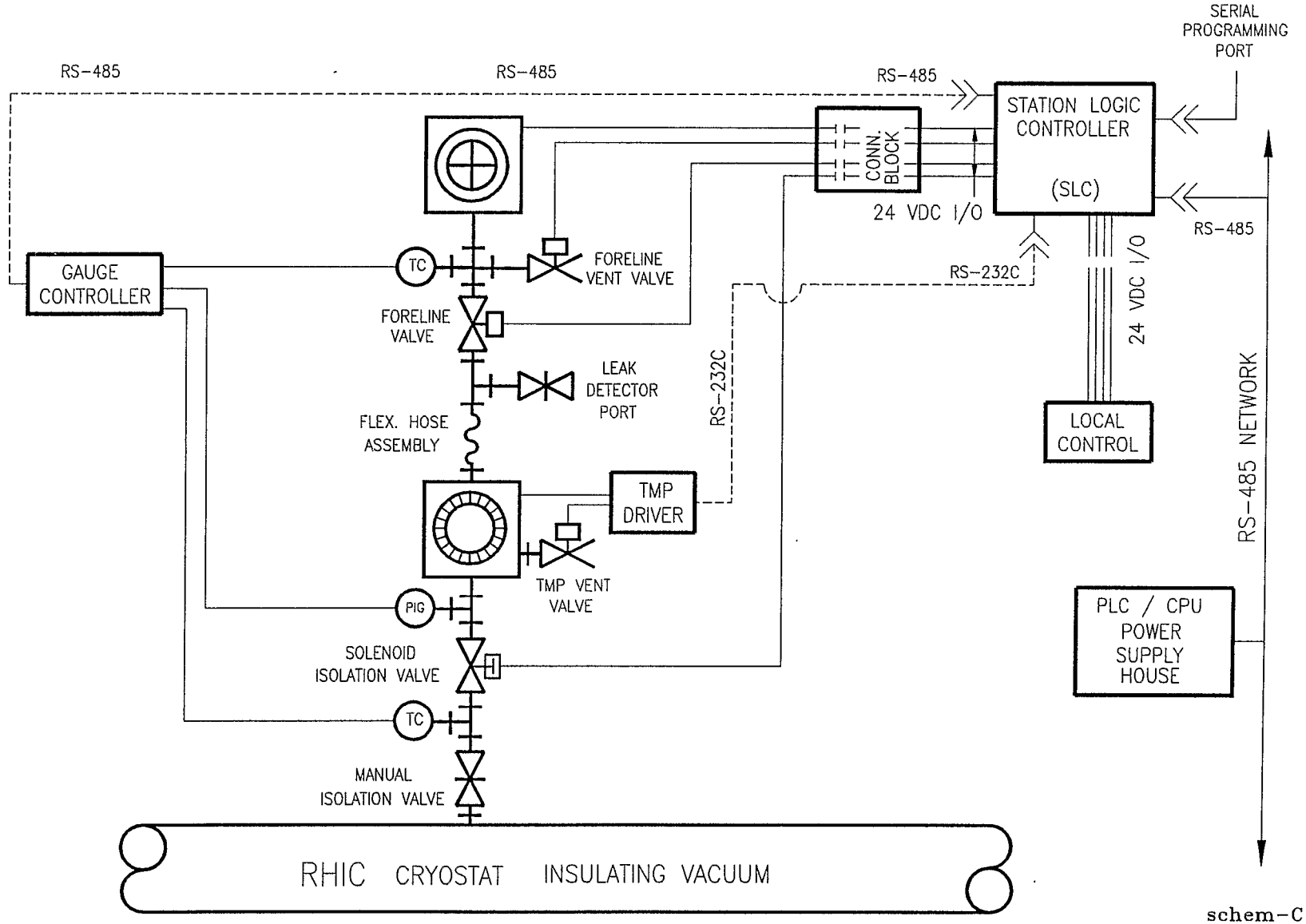

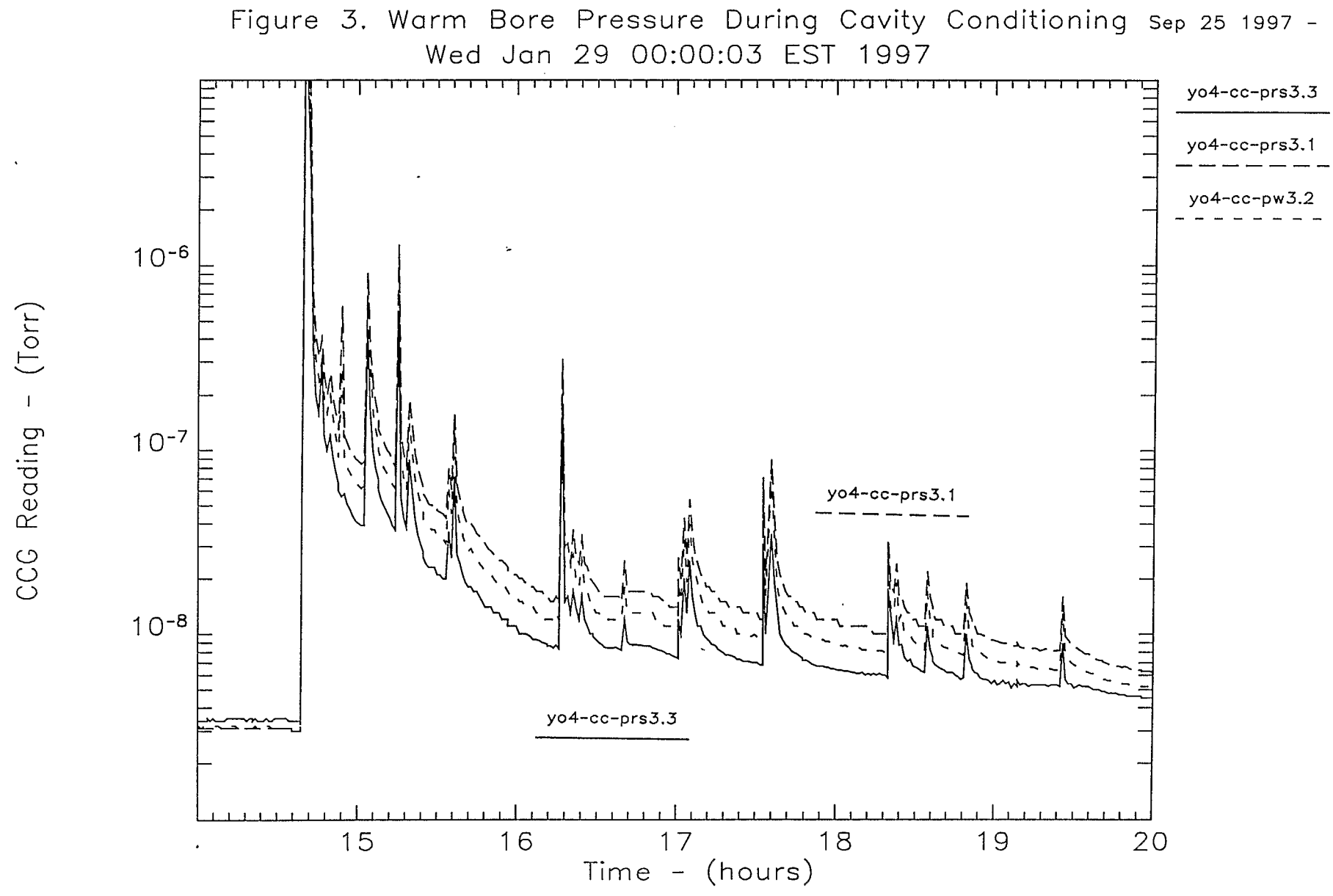
Figure 3. Warm Bore Pressure During Cavity Conditioning Sep 25 1997 - 1013
Wed Jan 29 00:00:03 EST 1997
yo4-cc-prs3.3
yo4-cc-prs3.1
yo4-cc-pw3.2
CCG Reading - (Torr)
10-6
10-7
10-8
yo4-cc-prs3.1
yo4-cc-prs3.3
15
16
17
18
19
20
Time - (hours)

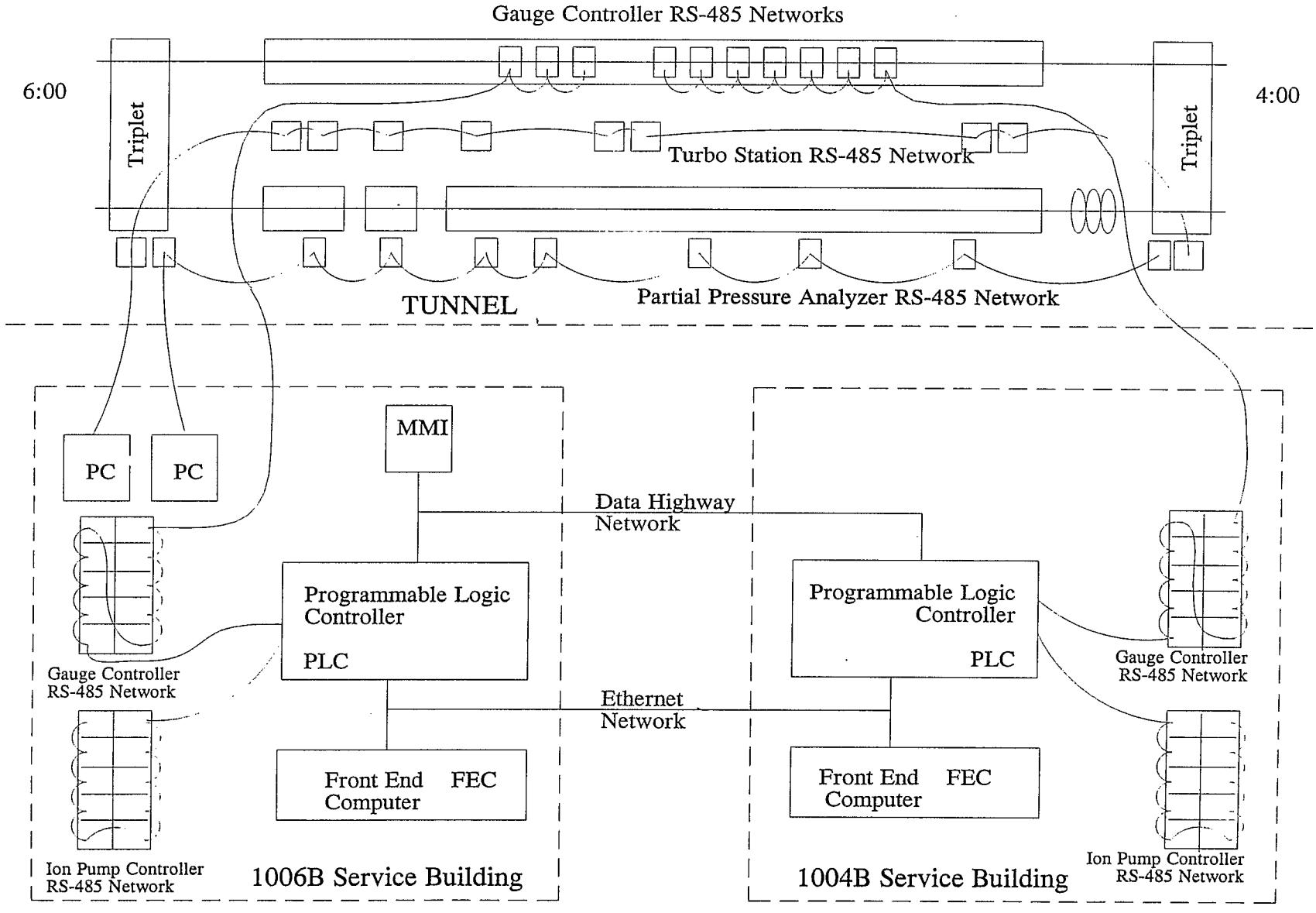

Figure 4. RHIC First Sextant Vacuum I & C System

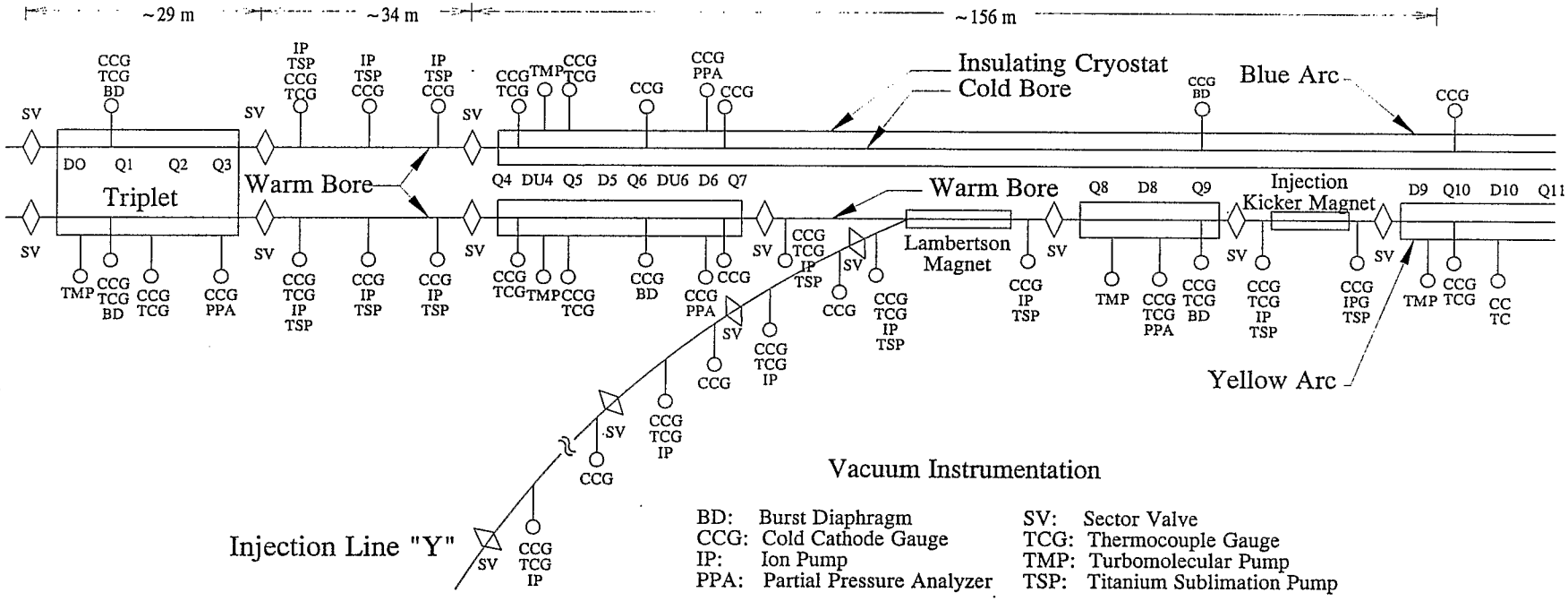

Figure 5. Layout of the First Sextant Vacuum Instrumentation, Injection Area.

Figure 6. Room Temperature Helium Gradient

Return Pressure on Yellow Arc Utility Line

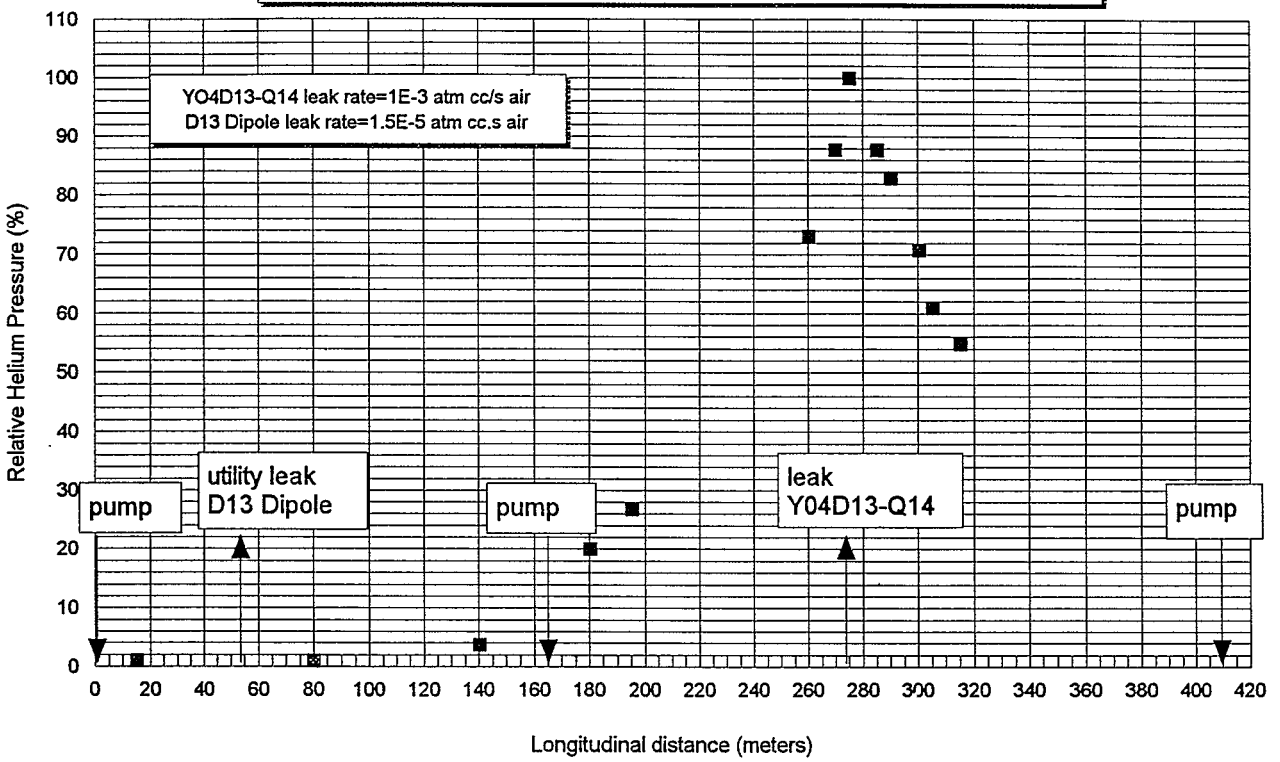

Figure 7. Cold Helium Gradient

Gradient Subsequent to YO4D13-Q14 Utility Line Repair

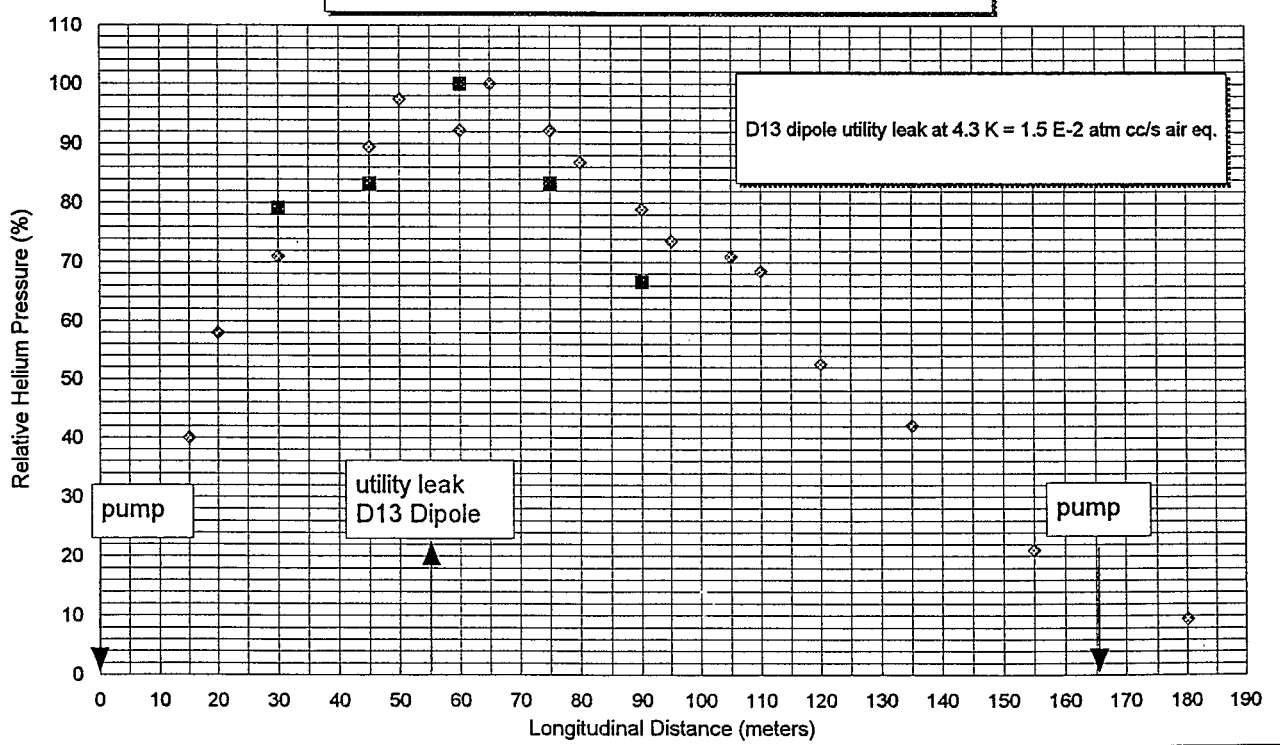

Figure 8. Cold Helium Gradient

Existing Utility Leak (1.5E-2 atm cc/s air eq) with Contrived Leak

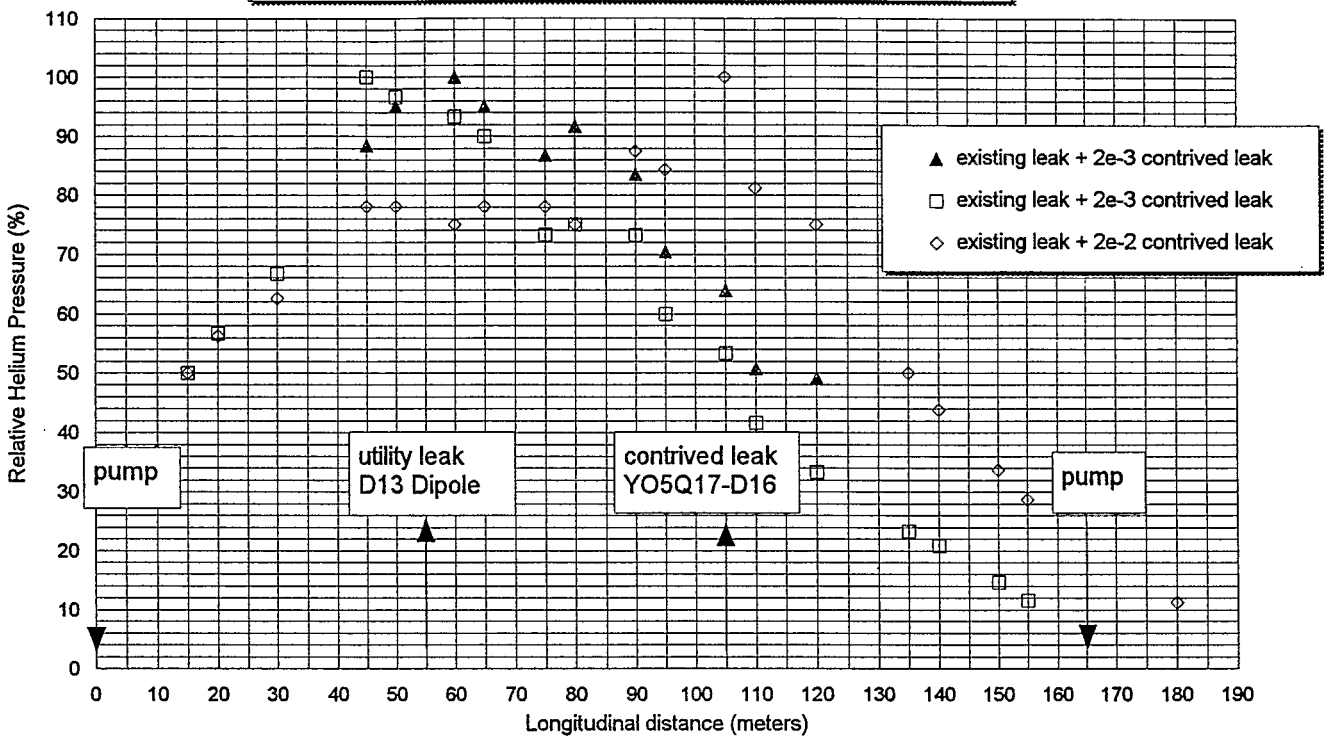

Figure 9. Helium Capacity of YO5Q8Q9 Cryostat

Outfitted with ~400 cm^2 Coconut Activated Charcoal

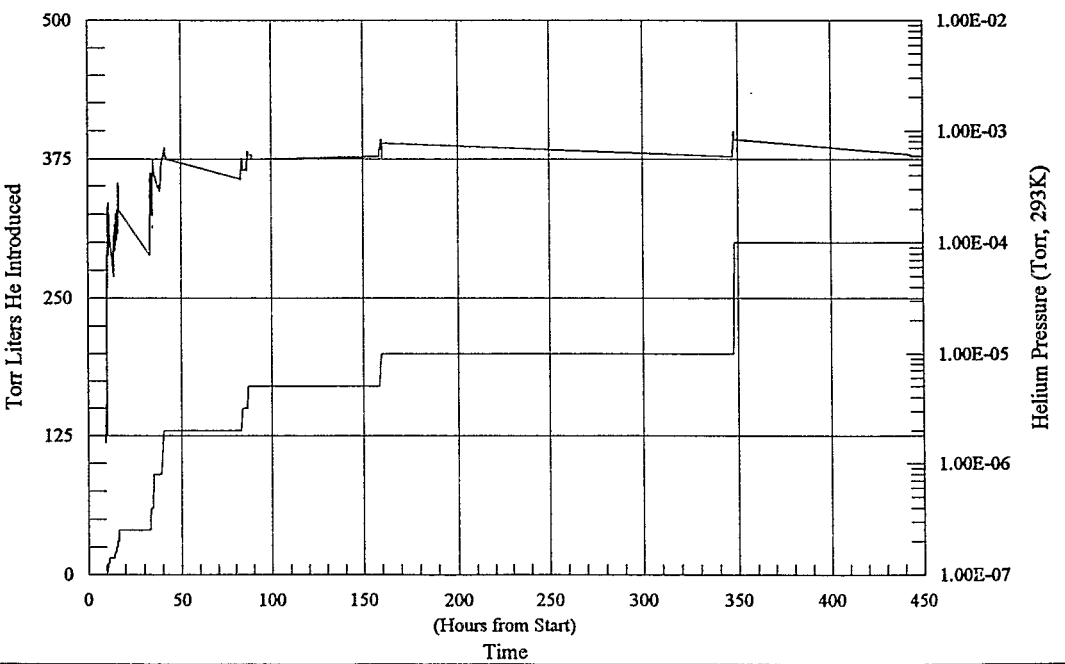

Figure 10. Helium Capacity of FST Cryostat vs Full Cell 2 Cryostat

Outfitted with ~460 cm^2 Coconut Activated Charcoal

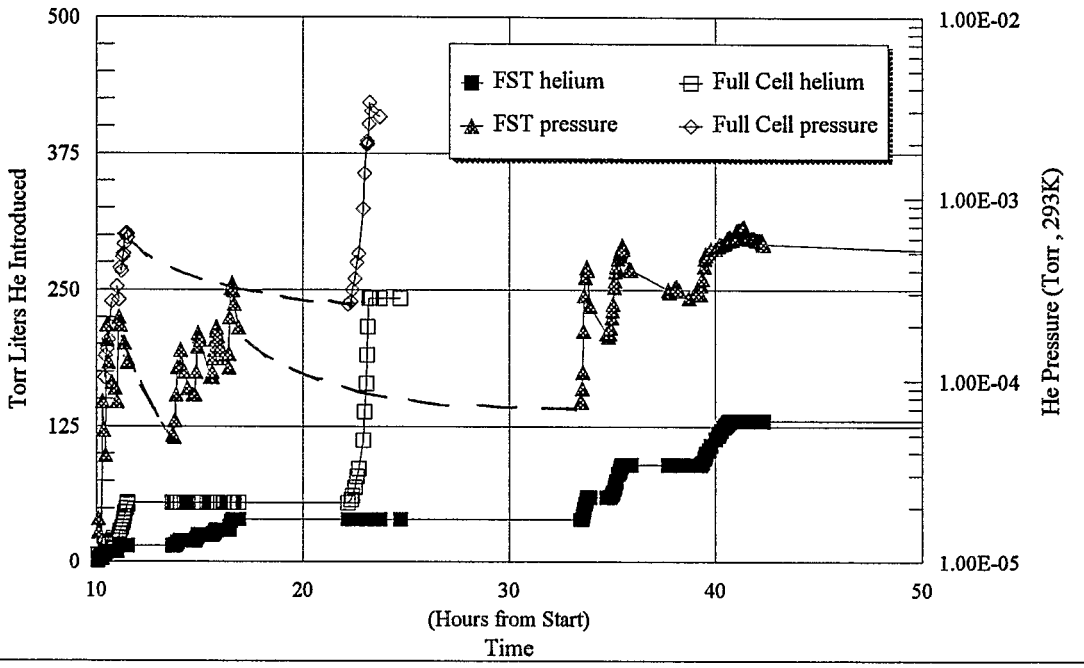

Figure 11. Cryostat Pressure vs Helium

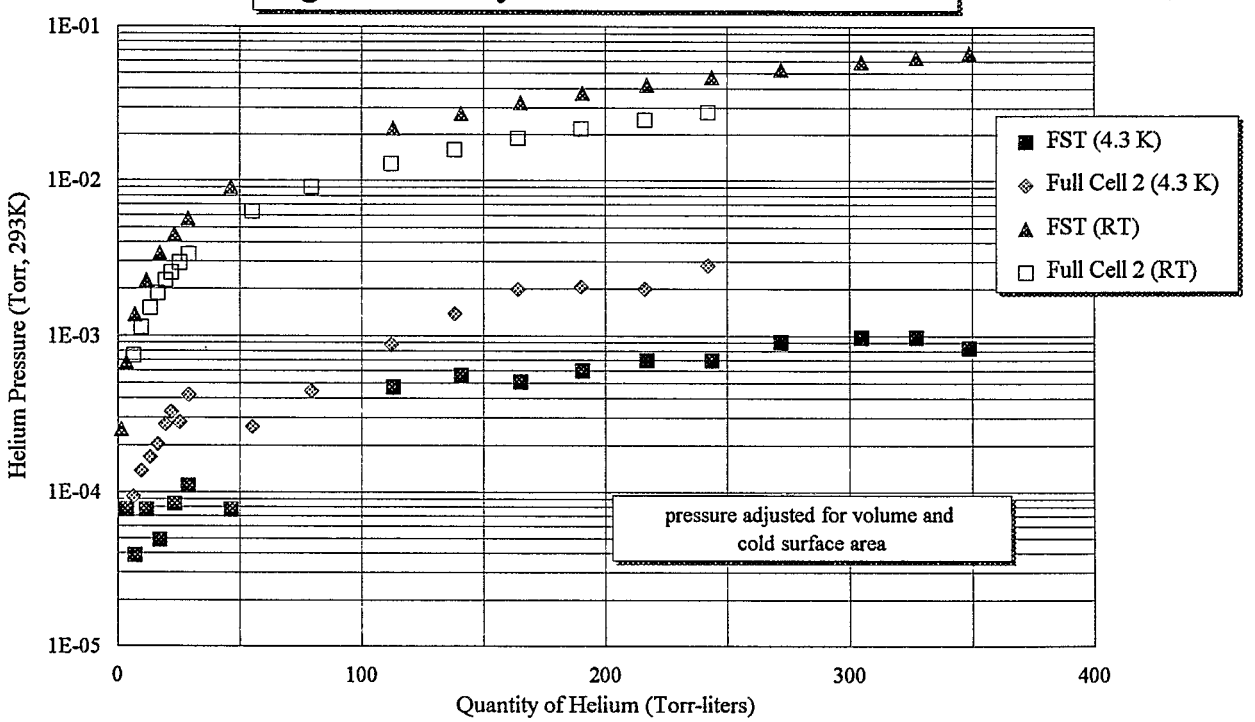

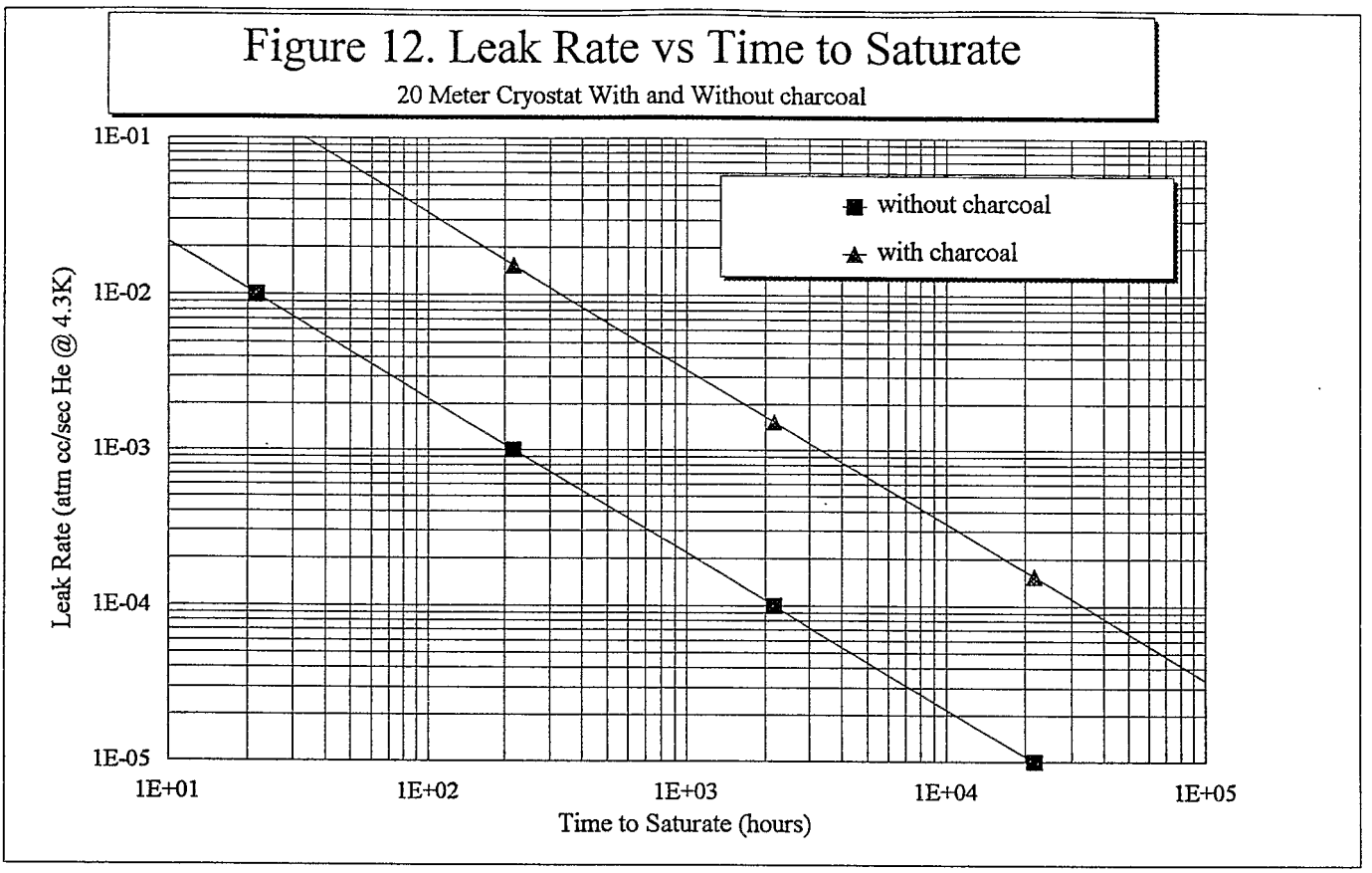

Figure 13. Cold Bore Spatial Layout

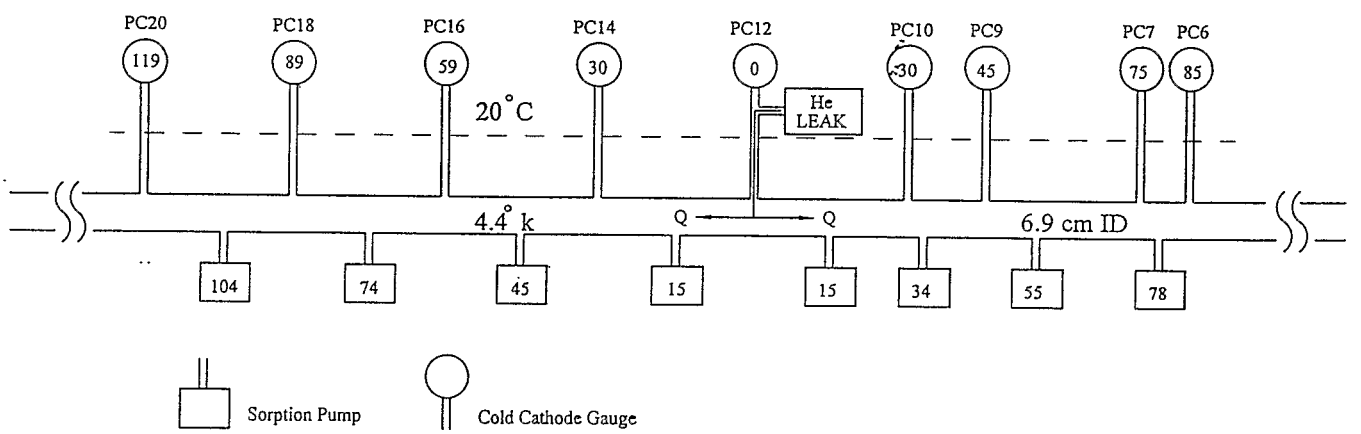

Figure 14. Cold Bore Pressure Toward 4:00 with He Leak-In

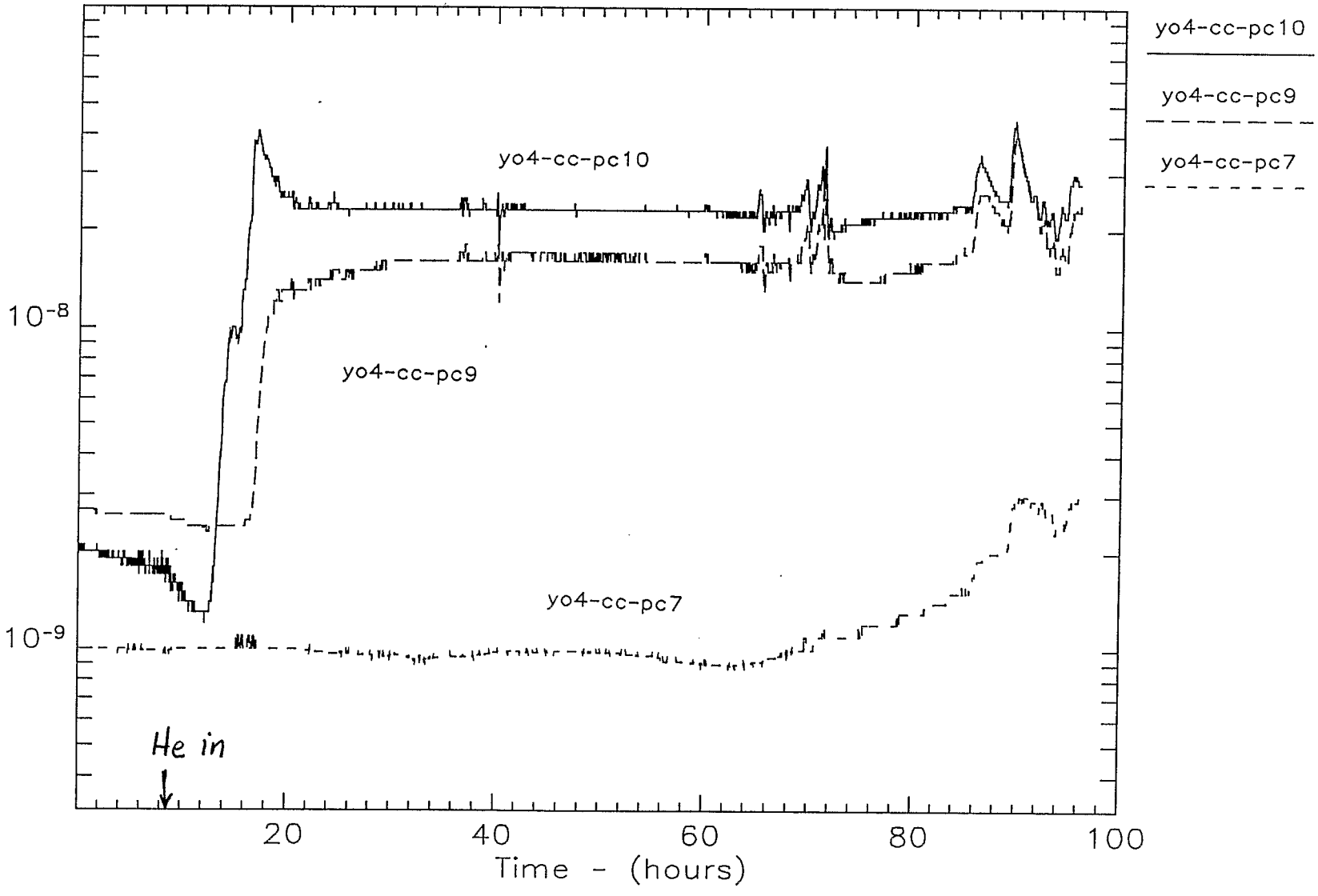

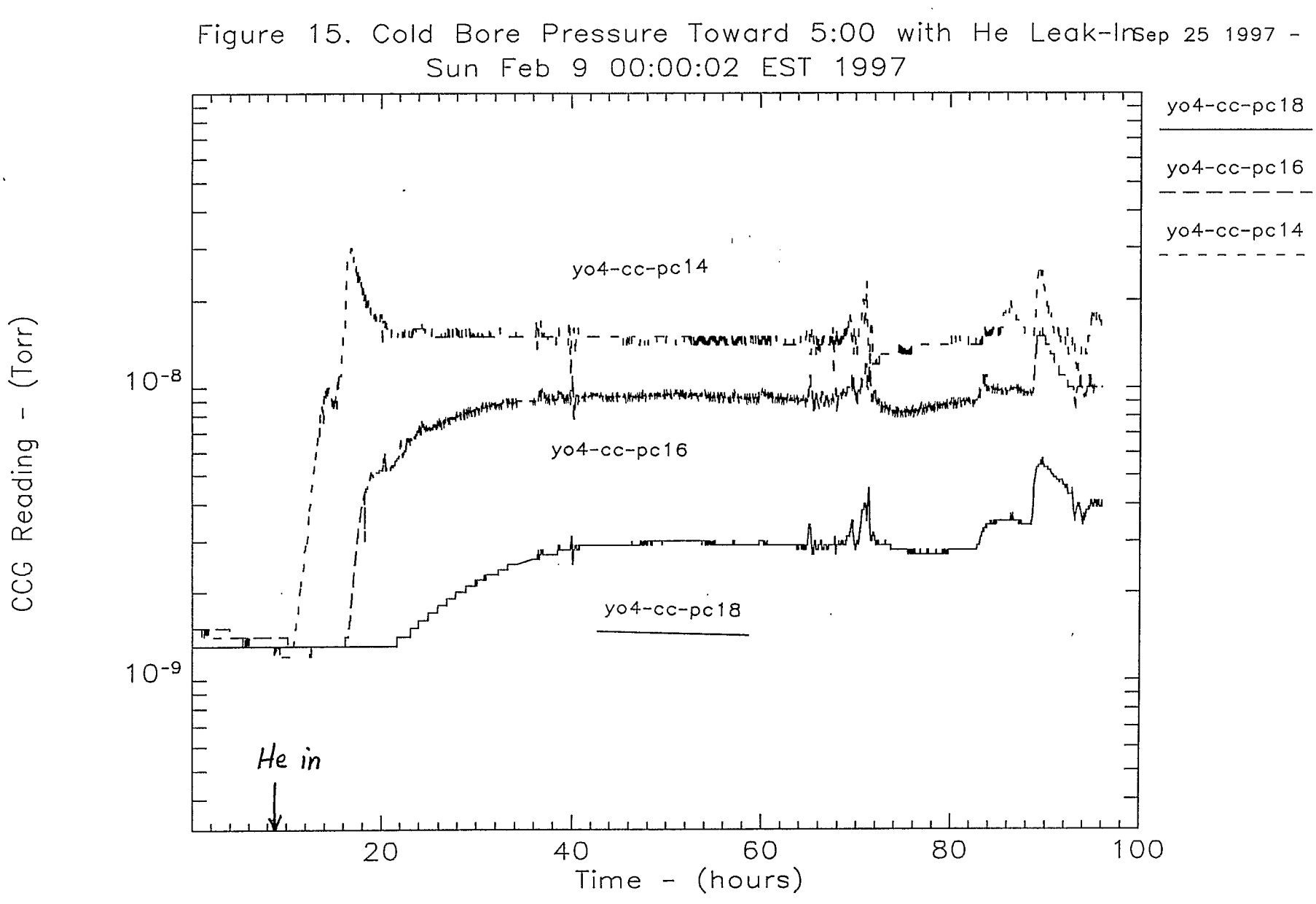
Figure 15. Cold Bore Pressure Toward 5:00 with He Leak-In
Sun Feb 9 00:00:02 EST 1997
Sep 25 1997 - 1009
yo4-cc-pc18
yo4-cc-pc16
yo4-cc-pc14
yo4-cc-pc14
yo4-cc-pc16
yo4-cc-pc18
10^{-8}
10^{-9}
He in
20
40
60
80
100
Time - (hours)
CCG Reading - (Torr)

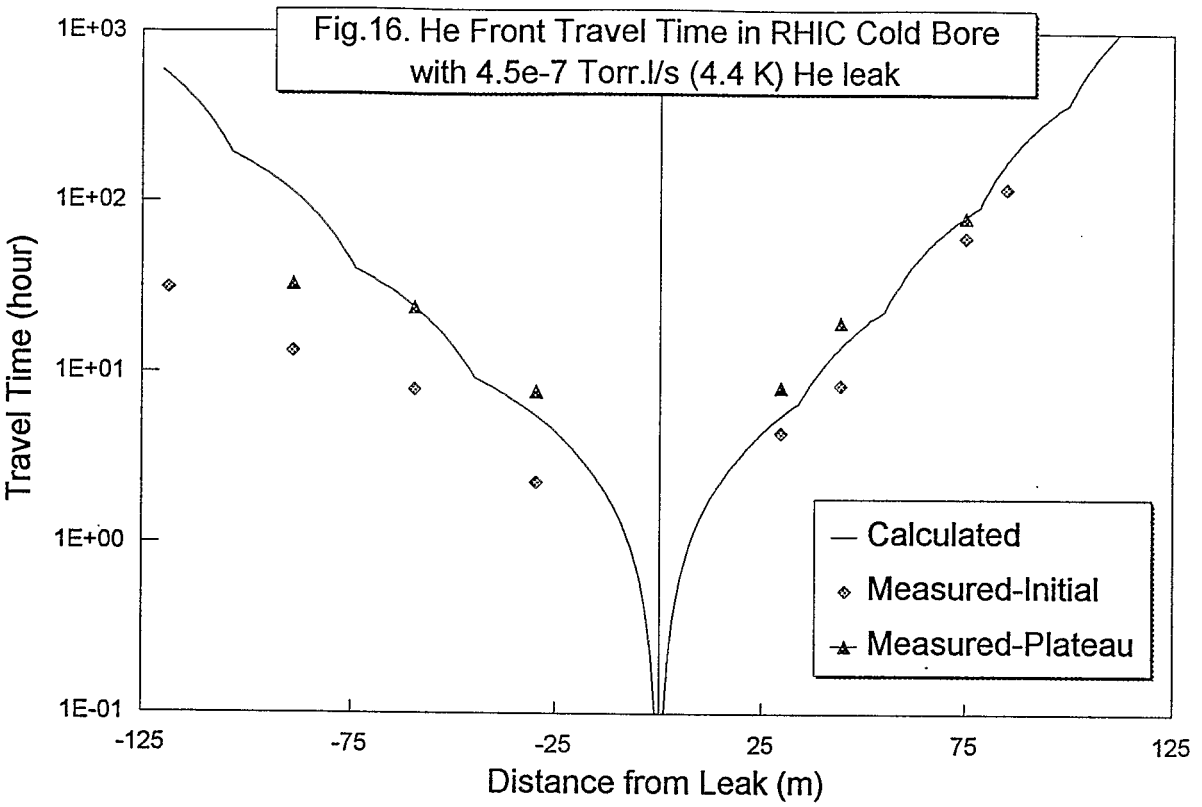
Fig.16. He Front Travel Time in RHIC Cold Bore
with 4.5e-7 Torr.l/s (4.4 K) He leak
Travel Time (hour)
1E+03
1E+02
1E+01
1E+00
1E-01
-125
-75
-25
25
75
125
Distance from Leak (m)
Calculated
Measured-Initial
Measured-Plateau

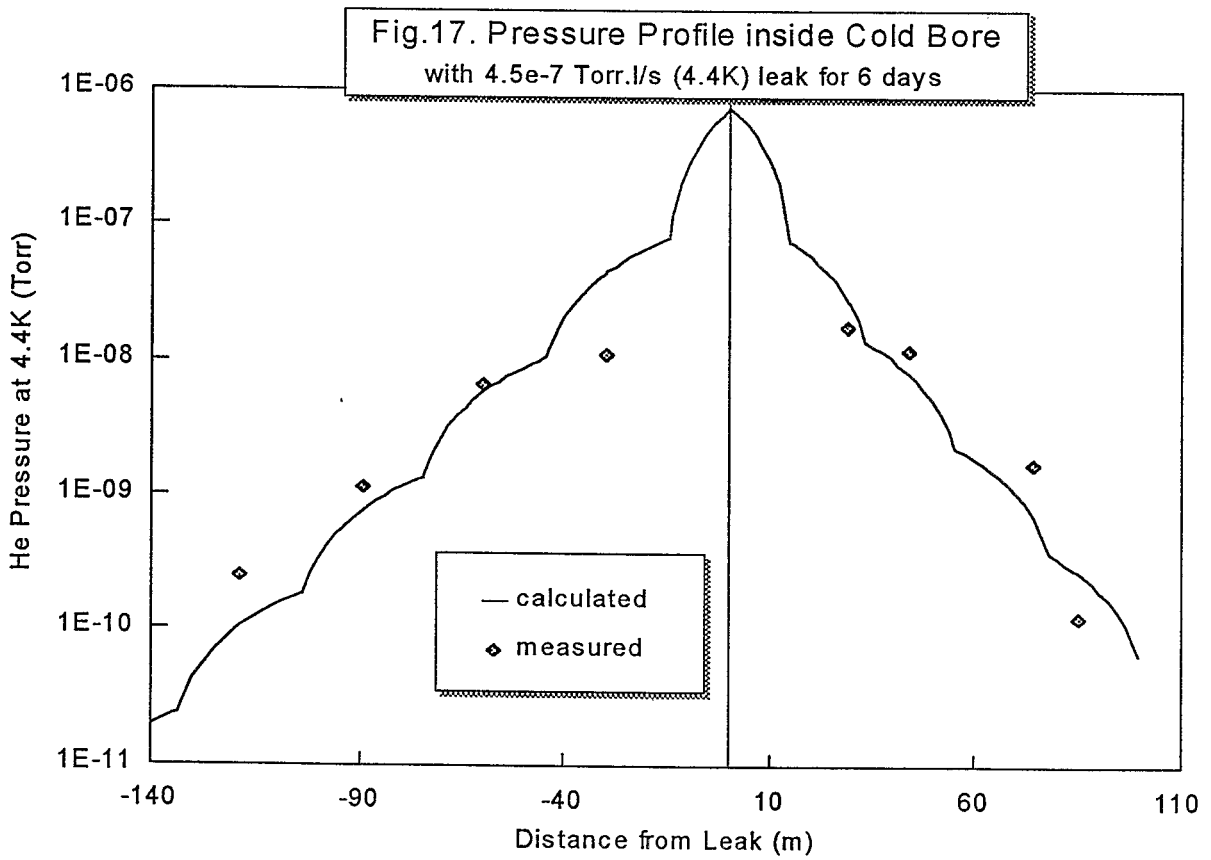
Fig.17. Pressure Profile inside Cold Bore
with 4.5e-7 Torr.l/s (4.4K) leak for 6 days
He Pressure at 4.4K (Torr)
1E-06
1E-07
1E-08
1E-09
1E-10
1E-11
-140
-90
-40
10
60
110
Distance from Leak (m)
calculated
measured